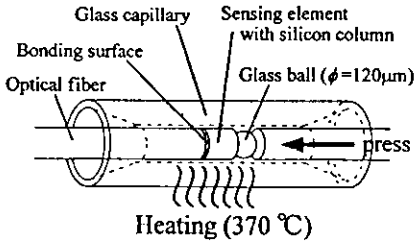


**Figure 4.** Schematic of the bonding process of sensing element to optical fiber end.

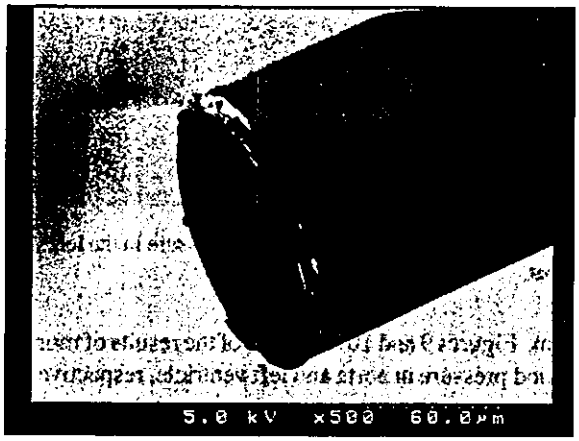


**Figure 5.** SEM photograph of fabricated pressure sensor of 125 $\mu$m in diameter.

can be obtained from a 4 inch silicon wafer. As this miniature pressure sensor can be produced at relatively low cost, it is suitable for disposable use, which is efficient for use in blood vessels.

A cleaved fiber end is coated with chromium by evaporation to make the half-mirror. The thickness of the chromium layer is about 10 nm. A metal half-mirror is optically neutral, which means that the reflectance and the transmittance do not depend on wavelength for a wide range. Therefore, it is effective for white light interferometry to achieve a linear sensor output.

The process of bonding the sensing element with silicon column to the half-mirror-coated optical fiber end is carried out in a glass micro capillary as a guide as shown in figure 4. The silicon column keeps the sensing element parallel to the fiber end in the glass capillary. The inner diameter of the capillary is 127 $\mu$m. The sensing element with silicon column and a micro glass ball of 120 $\mu$m in diameter are inserted into the capillary. The half-mirror-coated optical fiber is inserted into the capillary so as to face the sensing element. The other optical fiber is inserted from the other side and presses the polyimide layer of the sensing element on the fiber end. After confirming that the spectrum of the reflection light of the sensor is clearly observed, the capillary is heated stepwise up to 370 °C to bond the sensing element with silicon column to the fiber end.

After the bonding process, the silicon column is fully removed by $XeF_2$ etching. Figure 5 shows an SEM photograph of the completed sensor. The ultra-miniature sensing element at the fiber end can be observed.

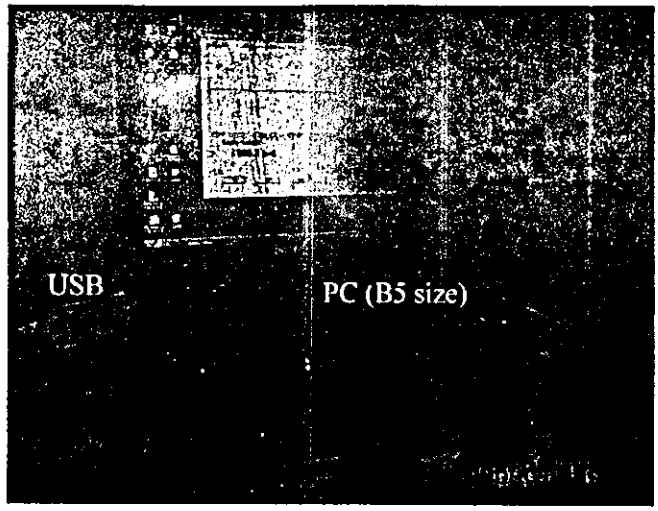


**Figure 6.** Photograph of developed fiber-optic pressure sensor system.

## 4. Experimental setup

The experimental setup of the developed sensor system is the same as shown in figure 1. The white light generated by a halogen lamp (OCEAN OPTICS, LS-1) reaches the sensor cavity and is modulated. The spectrum of the reflection light of the sensor cavity is detected by a miniature fiber-optic high-speed spectrometer (OCEAN OPTICS, USB2000). The captured spectrum data are transferred to a personal computer (PC) via a USB connection and are used to obtain the cavity length of the sensor. The cavity length is converted to a pressure value and then the pressure value is continuously displayed on the monitor of the PC. The sampling rate is about 70 Hz and it mainly depends on sampling at the spectrometer, the data transfer from the spectrometer to the PC. The developed sensor system is shown in figure 6. The white light source, the fiber coupler and the spectrometer are built into the box under the B5-size PC.

## 5. Experimental results

### *5.1. Measurement in a pressure-controlled chamber*

The fabricated fiber-optic pressure sensor was tested in a chamber connected to a pressure controller (NAGANO KEIKI, PC10). Figure 7 shows the reflection spectrum of the sensor for different pressures. Spectrum modulation was obtained and the peak shifts were clearly monitored. The measured cavity length using the spectrum data, as a function of applied pressure, is shown in figure 8. A least-squares fit of these data yields the sensitivity of $-0.25$ nm mmHg$^{-1}$ with the correlation coefficient having a value of 0.9993 and the resolution of 4 mmHg for pressures ranging from $-100$ to 400 mmHg. Averaging of the acquired cavity lengths calculated using more than one pair of peaks and interpolation between sampling data of pixels of the spectrometer contribute high resolution and low noise measurement. The resolution can be improved by noise reduction of the spectrometer or increasing the displacement of the diaphragm.

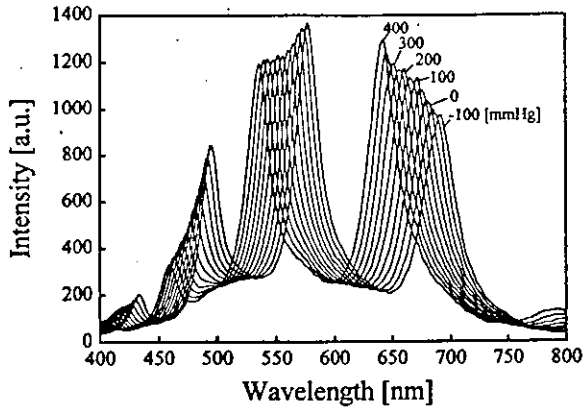


**Figure 7.** Reflection spectrum of developed pressure sensor for different applied pressures.

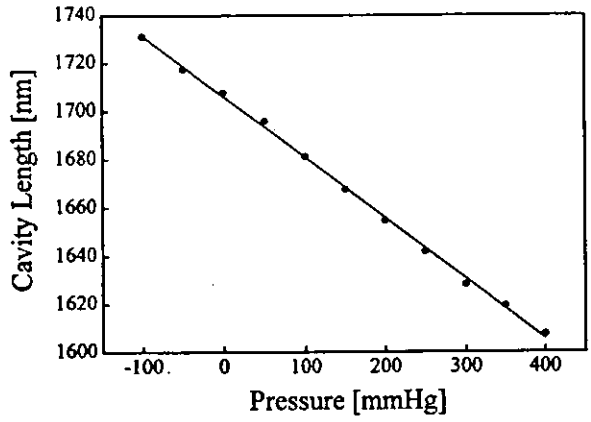


**Figure 8.** Detected sensor cavity length as a function of pressure.

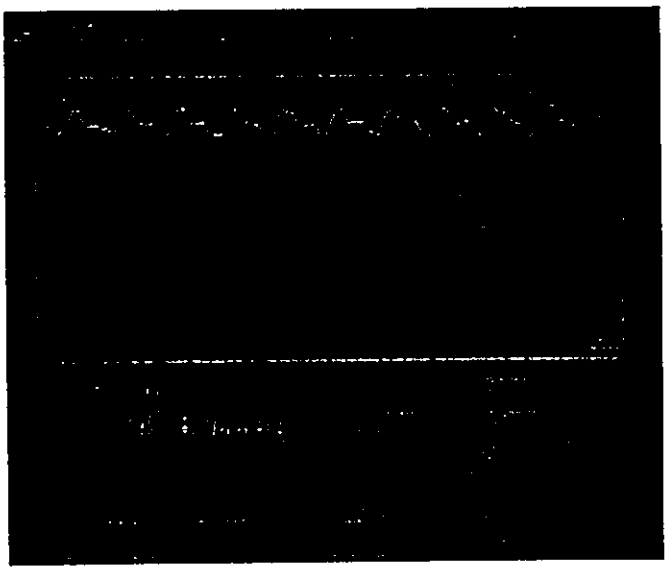

**Figure 9.** Continuous display of blood pressure in the aorta of a goat.

### *5.2. Experiments on animals*

Experiments on animals have been carried out. The developed sensor system was applied for monitoring blood pressure in the left ventricle, left atrium, right atrium and aorta of a goat. The ultra-miniature fiber-optic pressure sensor was set in an injection needle of which the outer diameter was about

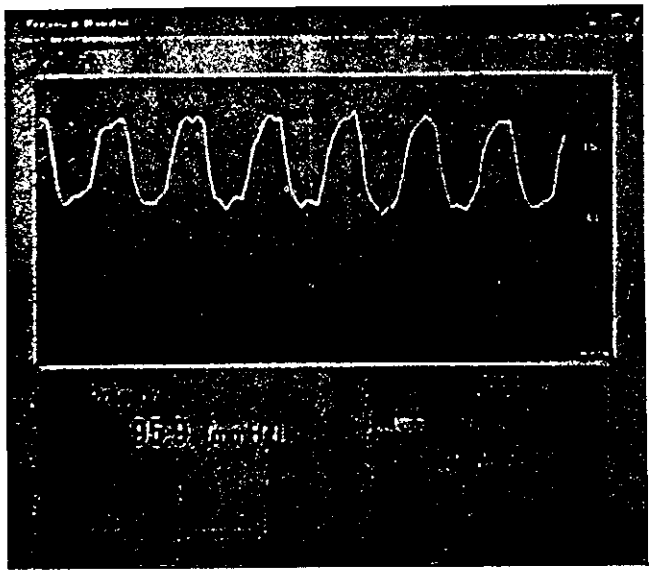

**Figure 10.** Continuous display of blood pressure in the left ventricle of a goat.

0.6 mm. Figures 9 and 10 show one of the results of monitoring the blood pressure in aorta and left ventricle, respectively. The pressures were successfully monitored and the waveforms of the dynamic pressure change were clearly observed.

## 6. Discussion

Owing to the low sampling frequency of the sensor system, disturbed waveforms of pressure have been observed. The sampling frequency depends on the data transfer rate from the spectrometer to the PC. A microcontroller-based spectrometer is suitable for increasing the data transfer rate for realizing higher sampling frequency utilizing parallel data processing.

During the pressure measurements, the influence of temperature change on the sensor output was observed. Specifically, the zero level of the sensor output depends on the ambient temperature. The problem is caused by expansion of the air in the sensor cavity [9]. For monitoring pressures *in vivo* (i.e., in a human body or in an animal), the temperature change can be neglected but careful calibration is required before monitoring in a medium the temperature of which is the same as that of the monitoring area. To avoid thermal drift, a packaging process using soldering to keep the sensor cavity in vacuum has been proposed and the development is on going [15]. Such an absolute sensor will be necessary for long-term monitoring.

Considering the sensitivity of the sensor, the low visibility of the reflection spectrum of the sensor, shown in figure 7, degrades the sensitivity. The extent of the light beam from the multimode fiber end at the sensor causes the geometric path difference and degrades the sensitivity. Although making the cavity length of the sensor small (about 2 $\mu$m in our sensor) reduces the effect of the path difference, it limits the increase of sensitivity because of the large numerical aperture (NA) of the multimode fiber. Consequently, utilizing a single-mode fiber the NA of which is smaller than that of the multimode fiber can increase the sensitivity. Moreover, the beam diameter of the light from the single-mode fiber end is smaller. Therefore,

a smaller mirror and a larger deformable area of the diaphragm can be designed to improve the sensitivity of the sensor. The fabrication process is exactly the same because the multimode and the single-mode fibers have the same outer diameter.

For clinical use, the sensor must be packaged in suitable medical tools (e.g., catheter, guide wire, needle) depending on the purpose. This sensor can be packaged in small medical tools because the diameter of the sensor is extremely small. Furthermore, it is an advantage that the function of the tools can be maintained even though the pressure sensor is embedded in one. We will examine not only fundamental sensor characteristics (e.g., thermal drift) but the packaging and the biocompatibility as well. In particular, the surface of the pressure sensor should be coated with suitable material to achieve biocompatibility for long-term monitoring.

From an economical viewpoint, even the spectrometer, which is the most expensive component in the sensor system, is available at a comparable price to a normal laptop PC. Consequently, the sensor system can be provided at a relatively low cost.

## 7. Conclusion

We have developed an ultra-miniature fiber-optic pressure sensor system for medical applications. The diameter of the sensor is 125 $\mu$m. A Fabry–Perot cavity is formed at the optical fiber end and a deformation of the diaphragm induced by pressure varies the cavity length. The sensing element is bonded to the optical fiber end utilizing a ring-shaped polyimide layer. White light interferometry is adopted to reduce error and noise caused by bending of the optical fiber and fluctuation of the light source. A measurement system for detecting the cavity length of the sensor has been developed. The system directly detects the modulated spectrum of the reflection light from the sensor interferometer using a commercial high-speed spectrometer. By tracking the shift of the peak wavelengths of the spectrum, the cavity length is calculated and the measured pressure is continuously displayed. Pressure has been successfully monitored in the heart and artery of a goat in real time using the developed sensor system.

Because of the ultra-miniature sensor head, this sensor can be used in a small-diameter blood vessel or a stenosed vessel. It can also be utilized for multi-point measurement at the same time by setting more than one sensor in a tool. Furthermore, the sensor is expected to be useful in multi-functional interventional tools.

## Acknowledgments

The authors would like to thank Professor T Yambe and Dr Y Shiraishi for help with experiments on animals. This work was supported in part by a Health and Labour Science Research Grants (Research on Advanced Medical Technology) from the Ministry of Health, Labour and Welfare of Japan. The authors acknowledge the support of Tohoku University 21COE Program 'Future Medical Engineering Based on Bio-nanotechnology'.

## References

[1] Wolthuis R A, Mitchell G L, Saaski E, Hartl J C and Afromowitz M A 1991 Development of medical pressure and temperature sensors employing optical spectrum modulation *IEEE Trans. BME* **38** 974–81

[2] Kalvesten E, Smith L, Tenerz L and Stemme G 1998 The first surface micromachined pressure sensor for cardiovascular pressure measurements *Proc. 11th IEEE Micro Electro Mechanical Systems (Heidelberg, Germany, 1998)* pp 574–9

[3] Tohyama O, Kohashi M, Sugihara M and Itoh H 1998 A fiber-optic pressure microsensor for biomedical applications *Sensors Actuators* A **66** 150–4

[4] Melvas P, Kalvesten E and Stemme G 2002 A temperature compensated dual beam pressure sensor *Sensors Actuators* A **100** 46–53

[5] Abeysinghe D C, Dasgupta S, Jackson H E and Boyd J T 2002 Novel MEMS pressure and temperature sensor fabricated on optical fiber *J. Micromech. Microeng.* **12** 229–35

[6] Rao Y J and Jackson D A 1994 A prototype fibre-optic-based Fizeau medical pressure and temperature sensor system using coherence reading *Meas. Sci. Technol.* **5** 741–6

[7] Haga Y, Minami K, Shoji S, Nitta S, Tanaka M and Esashi M 1994 A fiber-optic ultra miniature pressure sensor *Proc. 12th Sensor Symp. (Osaka, Japan, 1994)* pp 135–8

[8] Katsumata T, Haga Y, Minami K and Esashi M 2000 Micromachined 125 $\mu$m diameter ultra miniature fiber-optic pressure sensor for catheter *Trans. IEEJ* **120-E** 58–63

[9] Totsu K, Minh P N, Haga Y and Esashi M 2002 Development of ultra miniature fiber-optic blood pressure sensor system *Proc. 19th Sensor Symp. (Kyoto, Japan, 2002)* pp 429–32

[10] Bhatia V, Sen M B, Murphy K A and Claus R O 1996 Wavelength-tracked white light interferometry for highly sensitive strain and temperature measurements *Electron. Lett.* **32** 247–9

[11] Belleville C and Duplain G 1993 White-light interferometric multimode fiber-optic strain sensor *Opt. Lett.* **18** 78–80

[12] Rao Y J and Jackson D A 1996 Recent progress in fibre optic low-coherence interferometry *Meas. Sci. Technol.* **7** 981–99

[13] Chen S, Palmer A W, Grattan K T V and Meggitt B T 1992 Digital signal-processing techniques for electronically scanned optical-fiber white-light interferometry *Appl. Opt.* **31** 6003–10

[14] Lee C E and Taylor H F 1991 Fiber-optic Fabry–Perot temperature sensor using a low-coherence light source *J. Light. Technol.* **9** 129–34

[15] Totsu K, Haga Y and Esashi M 2003 Vacuum sealed ultra miniature fiber-optic blood pressure sensor using white light interferometry *Digest of Technical Papers of the 12th Int. Conf. on Solid State Sensors, Actuators and Microsystems: Transducers'03 (Boston, MA, 2003)* pp 931–4

JOURNAL OF APPLIED PHYSICS 97, 1 (2005)

# Synchronous rectification for contactless power supply utilizing Mn–Zn ferrite core coils

Hidekazu Miura,[a] Shinsuke Arai, Fumihiro Sato, and Hidetoshi Matsuki
*Graduate School of Engineering, Tohoku University, 6-6-05aza Aoba Aramaki Aoba ward Sendai, Miyagi 980-8579 Japan*

Tadakuni Sato
*NEC Tokin corporation*

(Presented on 11 November 2004)

Contactless power supply systems transmit electric power by electromagnetic induction with a pair of coils. The efficiency and the output voltage depend on parameters of coils. We studied the best parameter values that realize stable high efficiency contactless power supply. In the application with low output voltage, the voltage drop of the diodes becomes dominant power loss. A synchronous rectification was proposed as a solution of this problem. Our contactless power supply system for an artificial heart operates at 190 kHz. We use planar coils with Mn–Zn ferrite cores. Highly stable output voltage and 88% maximum efficiency were realized. © *2005 American Institute of Physics.*
[DOI: 10.1063/1.1850852]

## I. INTRODUCTION

Contactless power supply systems transmit electric power by electromagnetic induction with a pair of coils. The systems are applied to wireless power supply method for artificial organs to prevent recipients from infection syndromes and restraint of actions. We call thus a transcutaneous energy transmission system, TETS.[1,2] Also contactless power supply systems will make underwater vehicles free from wire and connectors. And we can use waterproof electronic product such as cellar phones or shavers.[3] The efficiency and the output voltage depend on parameters of self-inductance $L$ and mutual inductance $M$ of the coil. We studied the best parameter values that realize stable high efficiency contactless power supply. In the application with low output dc voltage, the voltage drop of the diodes becomes a problem of the loss. A synchronous rectification was proposed as a solution to this problem.

## II. DETERMINATION OF CIRCUIT PARAMETERS

Figure 1 shows the equivalent circuit of contactless power supply system. If the operating frequency is decided, the efficiency is calculated from the equivalent circuit

$$= \frac{R}{\dfrac{r_1\ r_2 + R^{\ 2} + {}^{2}L_2^{\ 2}}{{}^{2}M^{2}} + r_2 + R}.$$

$L$, $M$, and $r$ depend on the number $N$ of windings of coils. If we make coils with the uniform cross sections of coils, we can assume each parameter proportional to the square of $N$, then the efficiency is shown as functions of the number $T$ of windings of the secondary coil $C_2$=0 . The term, $n$ is the ratio of the winding number of the primary coil to the secondary coil. $L$ and $L$ are the values of one-turned self-inductances for the primary coil, and the secondary coil respectively. And $r$ and $r$ are the values of one-turned wire wound resistances for the primary coil and the secondary coil, respectively

$$L_1 = n^2T^2L,$$

$$L_2 = T^2L,$$

$$r_1 = n^2T^2r,$$

$$r_2 = T^2r,$$

$$N_1 = nT.$$

$T$, by which efficiency is assumed to be the maximum, is decided from this expression

$$T^4 \frac{rR^2}{r\ {}^{2}k^2LL^{\ 2} + rr + r\ \ {}^{2}k^2LL}.$$

The transformer formed by the coils is a loose-coupled one. This results in high output impedance and output variance. We use resonant capacitor $C_1$ in series. $C_1$ that minimizes internal impedance $Z_0$ is determined and the change of output voltage is suppressed when the load changes. In Fig. 2, the Helmholtz equivalent circuit is shown. In most cases, wire wound resistances $r_1$ and $r_2$ are negligible for output voltage considerations. $C_1$ is determined by

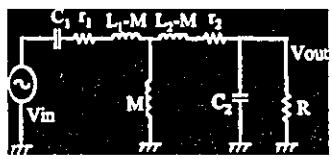


FIG. 1. Equivalent circuit of contactless power supply system.

[a]Author to whom correspondece should be addressed; electronic mail: biomg26@ec.ecei.tohoku.ac.jp

0021-8979/2005/97(10)/1/0/$22.50  

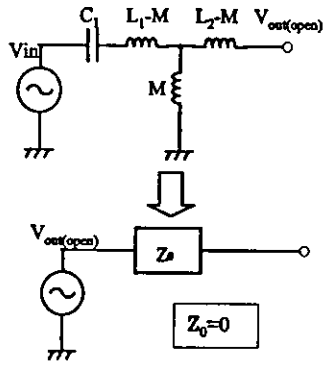


FIG. 2. Helmholtz equivalent circuit.

$$C_1 = \frac{1}{{}^2L_1\ 1\ \ k^2}.$$

The number $N_1$ of windings of primary coil is decided from ratio of the voltage

$$\frac{V_{\text{out open}}}{V_{\text{in}}}_{Z_0=0} = \frac{1}{k}\ \frac{\overline{L_2}}{L_1}.$$

In the common contactless power supply systems use detachable transformers. However, our goal is a more flexible power supply system; if the distance between coils or the location of coils changes, the coupling factor $k$ will vary and the minimum internal impedance condition will break. Setting $C_2$ to an appropriate value can stabilize the output voltage within the range of gap change. (see Fig. 3).

## III. SYNCHRONOUS RECTIFICATION

The synchronous rectifier circuit is shown in Fig. 4, where metal-oxide-semiconductor field effect transistor (MOSFETs) synchronize to the diodes. This operation reduces the diodes' voltage drops. Figure 5 shows wave forms of $V_1$, $V_2$, and gate voltages of $Q_3$, $Q_4$. When $V_1$ is higher than the threshold voltage *V*th of 3.5 V and $V_2$ is lower than *V*th, the gate control circuit turns MOSFETs $Q_1$ and $Q_4$ on. In the case where contrary $V_2$ is higher and $V_1$ is lower, it turns MOSFETs $Q_2$ and $Q_3$ on. Both $V_1$ and $V_2$ are lower than *V*th, which turns all the MOSFETs off. This operation has a very important role. The switching timings depend on diodes. This prevents the system from malfunctions, such as shoot-through conditions.

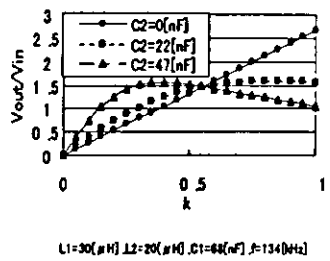


FIG. 3. Output voltage vs coupling factor $k$: 47 [nF] is the suitable value for $C_2$.

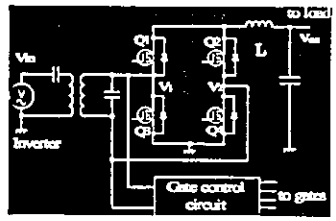


FIG. 4. Synchronous rectifier circuit.

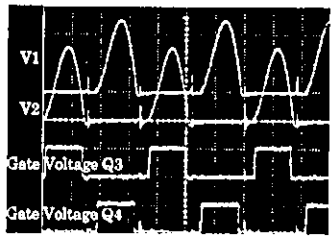


FIG. 5. Wave forms of the synchronous rectifier circuit.

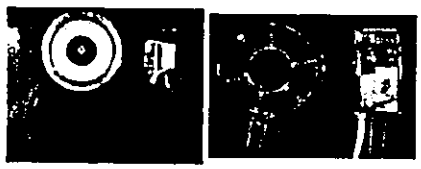

FIG. 6. Contactless power supply system for an artificial heart. Primary unit (left) has a 120-mm-diam coil and a high frequency inverter. Secondary unit (right) has 80-mm-diam coil and a synchronous rectifier unit that is 75 mm high, 40 mm wide and 16 mm thick.

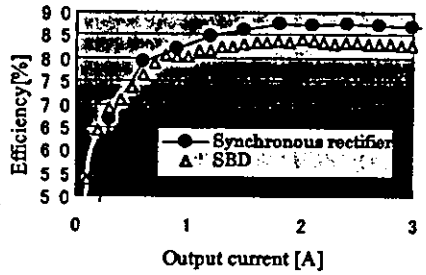


FIG. 7. Efficiency vs output current. Where 88% maximum efficiency (dc to dc) was achieved. The maximum efficiency of the system utilizing schottky barrier diodes is 84%.

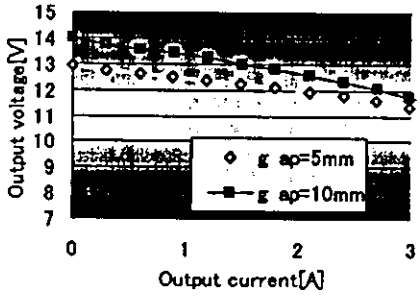


FIG. 8. Output voltage vs output current characteristics was measured at 5 and 10 mm distances between coils.

## IV. RESULTS AND DISCUSSION

In Fig. 6, the contactless power supply system we have developed for an artificial heart is shown.[4] This system operates at 190 kHz, and we use planar coils with Mn–Zn ferrite cores. The efficiency of the contactless power supply with synchronous rectifier is 88[%] maximum (dc-dc). Efficiency has been improved by four points compared with the one in which surface behavior diagram were used (Fig. 7). Under 3[A] output current, the output voltage varies 2.6 V . The output voltage is very stable (Fig. 8). We have period in which all the MOSFETs are off. In this period, current runs through the diodes, the loss increase and $V_1$ and $V_2$ are low at same time; this means voltage of the secondary coil is distorted. Improvement of the gate control circuit to reduce all MOSFETs off time is necessary. Power consumption of each component should be clarified. We are trying to eliminate the capacitor $C_2$ and the inductor $L$, because these are huge components.

## V. CONCLUSION

A method for systematic circuit parameter determination was examined. A contactless power supply system with synchronous rectifier was constructed. The system achieved 88% maximum efficiency and highly stable output voltage.

We still have the possibility of improving efficiency, because current runs through diodes in the long periods that all the MOSFETs are turned off. Also, we are making an effort to miniaturize the rectifier unit with the elimination of the huge inductor and resonant capacitor.

[1]J. C. Schuder, H. E. Stephenson, and J. F. Townsend, IRE Int. Conv. Rec. **9**, 119 (1961).
[2]H. Matsuki, K. Nadehara, T. Watanabe, K. Murakami, and T. Yamamoto, IEEE Trans. Magn. **25**, 3812 (1989).
[3]H. Sakamoto and K. Harada, IEEE Trans. Magn. **29**, 3228 (1993).
[4]Y. Abe, T. Chinzei, T. Isoyama, T. Ono, S. Mochizuki, I. Saito, K. Iwasaki, M. Ishimaru, T. Karita, A. Kouno, K. Baba, and K. Imachi, Artif. Organs **25**, 69 (2001).

*Artificial Organs*
28(2):226–237, Blackwell Publishing, Inc.


# Thoughts and Progress

## Development of an Electro-stethoscope System and Design of an Optimum Filter Based on Tissue Sound Transmission for Noninvasive Early Diagnosis of Malfunction of an Implanted Mechanical Total Artificial Heart

**Eiji Okamoto, †Taku Inoue, *Takuya Hashimoto, ‡Itsuro Saito, ‡Yusuke Abe, §Tsuneo Chinzei, §Takashi Isoyama, ‡Kou Imachi, and #Yoshinori Mitamura*
**Department of Electronics and Information Engineering, Graduate School of Engineering, Hokkaido Tokai University, Sapporo, Japan; †Department of Bioscience and Technology, School of Engineering, Hokkaido Tokai University, Sapporo, Japan; ‡Department of Biomedical Engineering, Graduate School of Medicine, University of Tokyo, Tokyo; §Research Center for Advanced Science and Technology, University of Tokyo, Tokyo; and #Department of System Information Engineering, Graduate School of Engineering, Hokkaido University, Sapporo, Japan*

**Abstract:** Early diagnosis of the malfunction of a mechanical artificial heart implanted in a patient who has been discharged from hospital is very important. We have developed an electro-stethoscope system that enables the malfunction of an artificial heart to be detected from the analysis of sound signals from the artificial heart. The sound data can be transmitted to a hospital via a mobile telephone or the Internet, so that doctors can examine the condition of the artificial heart. The optimum frequency characteristics of a low-pass filter for the elimination of ambient sound through the electro-stethoscope casing were obtained by simulating sound transmission through tissue. We evaluated the usefulness of the electro-stethoscope system using a goat in which an undulation pump total artificial heart had been implanted. A frequency analysis of the sound signal provided information on the degree of degradation of each mechanical component of the artificial heart. The results of this study showed that the electro-stethoscope system is useful for the early detection of the malfunction of an artificial heart at home, and that the use of the system contributes to improvement in the quality of life of patients. **Key Words:** Artificial heart—Electro-stethoscope—Telemedicine—Stethoscope—Tissue characteristics.

Received December 2002; revised March 2003.
Address correspondence and reprint requests to Dr. Eiji Okamoto, Department of Electronics and Information Engineering, Graduate School of Engineering, Hokkaido Tokai University, Minami-sawa 5-1-1-1, Minami-ku, Sapporo 005-8601, Japan. E-mail: okamoto@de.htokai.ac.jp

While a reliable method for the early detection of the malfunction of an implanted artificial heart is needed to ensure the safety of patients with implanted artificial hearts, an early diagnosis system of the implanted artificial heart has hardly been researched.

Sound signals generated by an artificial heart may be an index of the degree of mechanical deterioration, because characteristics of sound signals generated by an artificial heart are related to the condition of each mechanical component of the artificial heart (1,2). For detecting the malfunction of an artificial heart, we have developed an electro-stethoscope system, which enables sound from the artificial heart to be detected on the surface of the patient's body.

The object of this study was to demonstrate the feasibility of the newly-developed electro-stethoscope system by means of in vivo experiments using a total artificial heart (TAH).

### METHOD

The electro-stethoscope system consists of a pick-up microphone built into a commercially available stethoscope, an amplifier and a mobile computer. Sound data, which are detected on the surface of the body of a patient in whom a TAH has been implanted, are fed into the mobile computer via an A/D converter.

While tissue has the same frequency characteristics of sound transmission as that of a low-pass filter, the frequency components of the measured sound signal involve higher frequency components, which come from ambient sound around a patient.

In this study, we designed an optimum low-pass filter that has the same frequency characteristics as those of sound transmission through tissue, in order to eliminate the high-frequency noise signal. The theoretical relationship between the pressure of the sound source $P_0$ and the sound pressure $P_m$ measured by the microphone is given by

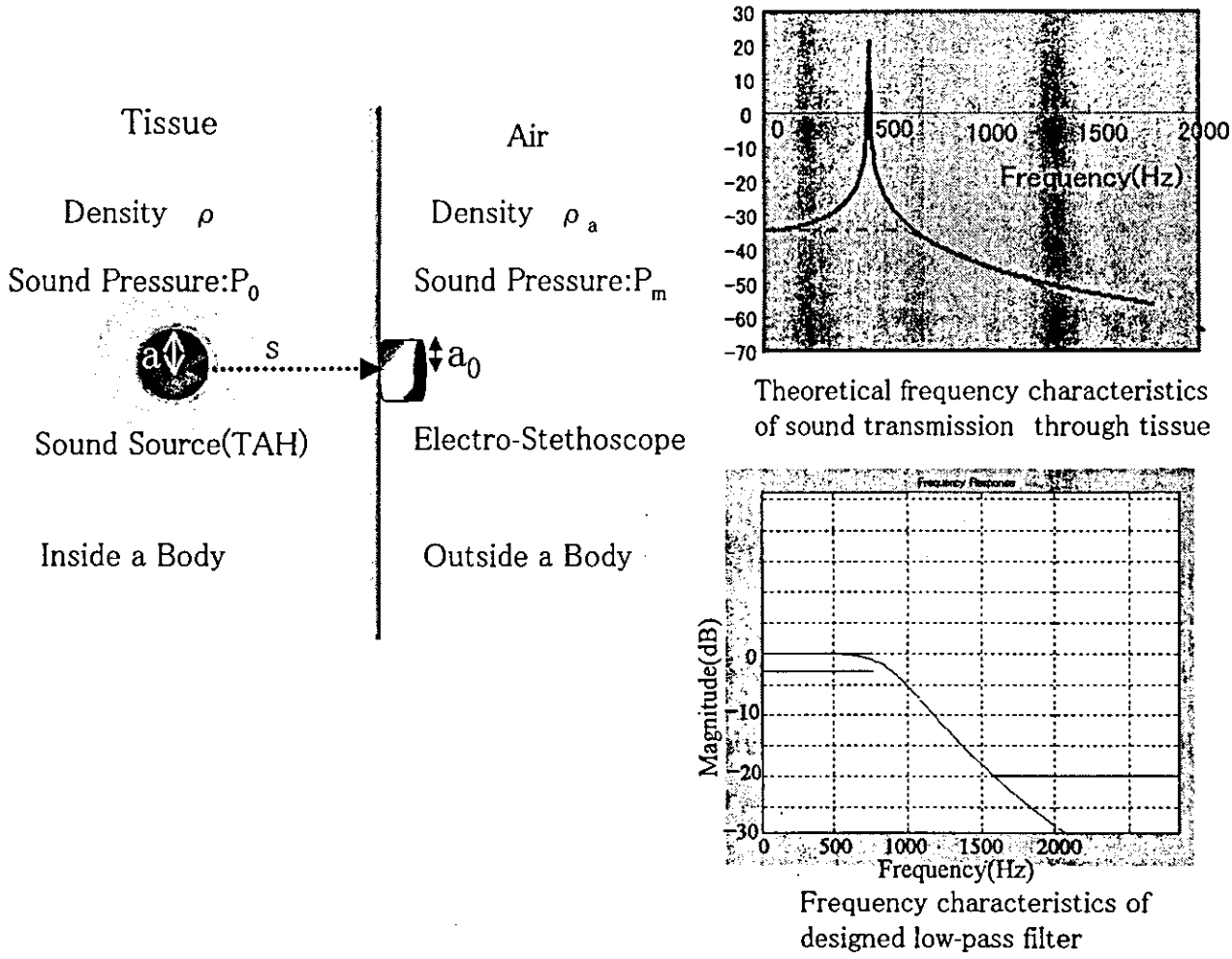


**FIG. 1.** Calculation results of the tissue characteristics of sound transmission, and a designed low-pass filter for the elimination of ambient sound.

$$\frac{P_m}{P_0} = \frac{0.8488 \cdot a}{s^2} \cdot \frac{1}{1-\left(f/f_c\right)^2} \quad (1)$$

$$f_c = \frac{1}{2\pi}\sqrt{\frac{\rho_a \cdot c_a^{\,2}}{0.4244 \cdot \rho \cdot a_0 \cdot d}}, \quad (2)$$

where the density of air is $\rho_a = 1.18$ kg/m$^3$, the density of tissue is $\rho = 1000$ kg/m$^3$, the sound velocity in air is $c_a = 340$ m/s, and the radius and heights of an air cavity of the microphone are $a_0 = 17$ mm and $d = 2$ mm (Fig. 1) (3). An undulation pump TAH (UPTAH) with a radius of 38 mm was used as the sound source a (4). The depth of the position of the UPTAH implantation was measured as $d = 170$ mm using a goat (body weight of 45 kg).

The frequency characteristics of a newly-designed low-pass filter using results of tissue frequency characteristics are also shown in Fig. 1. The cut-off frequency of the low-pass filter was designed to be 850 Hz, according to the frequency characteristics of sound transmission through tissue.

## RESULTS

The performance of the newly-developed electro-stethoscope system for the detection of the malfunction of an artificial heart was evaluated in in vivo experiments using an UPTAH. An UPTAH was implanted into a goat weighing 45 kg and was driven by an external controller through a percutaneous lead. Sound data were fed into a personal computer via an A/D converter (sampling frequency of 44 kHz, data length of 16 bits). Frequency components in the sound data were analyzed on a personal computer using signal processing software (Matlab, Cybernet System, Tokyo, Japan).

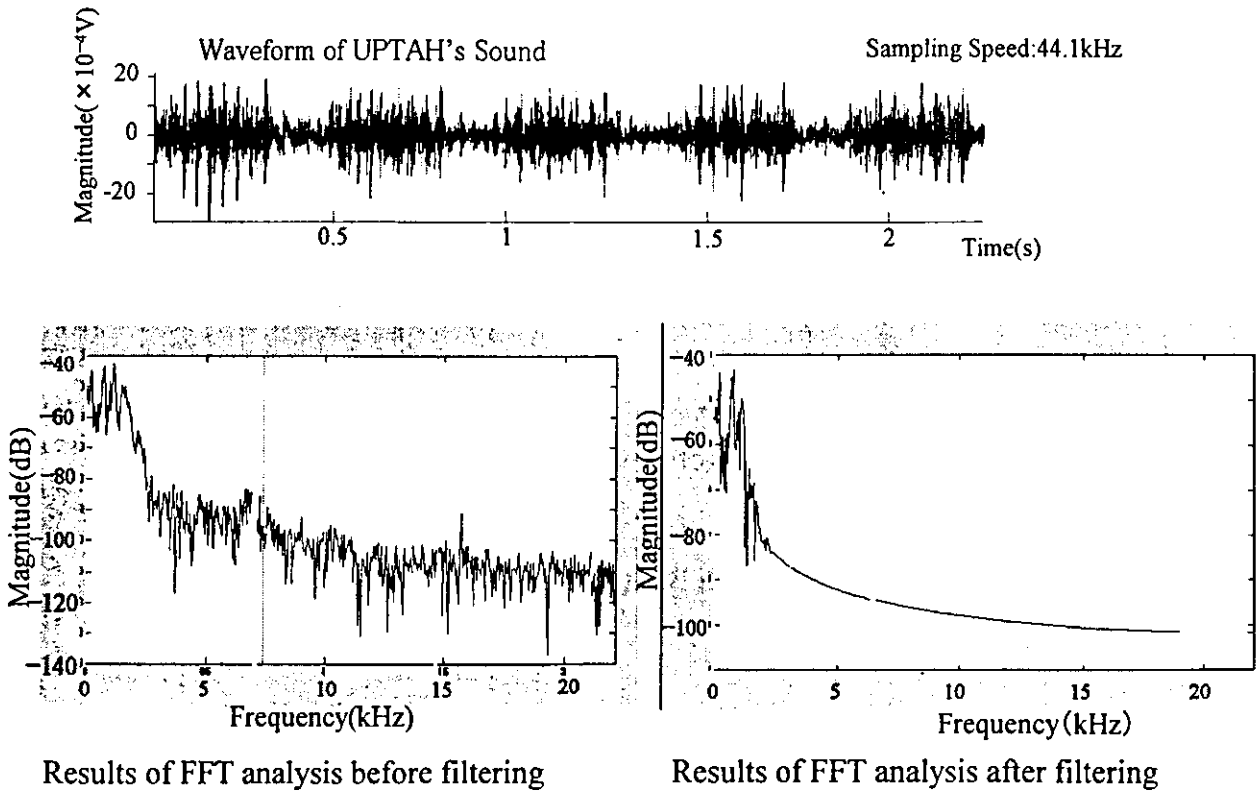


FIG. 2. UPTAH's sound signal and fast Fourier transform (FFT) analysis in animal experiments.

Figure 2 shows the measured waveform of the UPTAH's sound signal detected on the goat's body and the result of a frequency analysis during the higher motor velocity phase. While characteristics of sound transmission through the skin had that of a low-pass filter, as can been seen in Fig. 1, the measured sound signal included high-frequency components.

Figure 2 also shows frequency components of the sound data after eliminating high-frequency components by using a low-pass filter. The elimination of the high-frequency components of the signal enabled the sound of the UPTAH to be heard clearly, and it contributed to an improvement in the early diagnosis of mechanical malfunction in the UPTAH.

## DISCUSSION

Early detection of the malfunction of a mechanical artificial heart implanted in a patient who has been discharged from hospital is important because the malfunction of the implanted artificial heart may be fatal for the patient. However, an early diagnosis system for malfunctions has not been developed.

We have developed an electro-stethoscope system that enables the early detection of the malfunction of an implanted mechanical artificial heart. The motor current may also be a useful index for early detection of a malfunction, but motor current data only provide information on the overall degree of degradation of the artificial heart. Sound data provide information on the degree of degradation of each mechanical component of the artificial heart by means of investigating the change in each frequency component, because the frequency of sound and the vibration of each mechanical part depend on the rotational velocity and structure of each mechanical component (1,2).

Results of a fast Fourier transform (FFT) analysis showed that sound from the UPTAH includes a frequency component of 8.33 Hz and its harmonics, corresponding to a left motor speed of 500 rpm during the high-velocity phase. The sound also includes a frequency component of 13.3 Hz and its harmonics, corresponding to a right motor velocity of 800 rpm. Similar results were obtained during the low-motor-speed phase. The time series change of amplitude in each frequency component provides information on the degree of degradation of

each mechanical component of the artificial heart's actuator.

In this article, we have proposed a new design method for eliminating high-frequency noise in the sound from an artificial heart. Optimum characteristics of a low-pass filter can be obtained by simulating sound transmission through tissue. The newly-designed low-pass filter, whose cut-off frequency is 850 Hz, showed an improvement in the quality of the measured artificial heart sound, allowing doctors to detect a change in the condition of the artificial heart.

## CONCLUSION

We have developed an electro-stethoscope system for detecting the malfunction of an implantable artificial heart by means of measuring sound from the artificial heart on the surface of the patient's body. The results of this study showed that this electro-stethoscope system contributes to the early detection of a malfunction in the artificial heart of a patient, and also use of this system promises an improvement in the quality of life of a discharged artificial heart patient.

**Acknowledgments:** This study was supported in part by the program for the Promotion of Fundamental Studies in Health Science of the Organization for Drug ADR Relief, R&D Promotion and Product Review of Japan, and by a Grant-in-Aid for Scientific Research from the Japanese Ministry of Education, Science, Sports and Culture.

## REFERENCES

1. Okamoto E, Fujiyoshi M, Yoshida T, Mitamura Y, Mikami T. Development of PTFE coated ball bearing for implantable motor-driven artificial heart. *ASAIO J* 1996;42:5.
2. Okamoto E, Fujiyoshi M, Mitamura Y. Estimation of PTFE coated ball bearing for motor-driven artificial heart. *Jpn J Artif Organs* 1997;26:309–14.
3. Sasou K, Yagi S, Suzuki A, Nakayama K. Characteristics of the lung-sound microphone on the chest wall. *Trans Jap Soc Med Bio Eng* 1992;30:261–6.
4. Abe Y, Chinzei T, Isoyama T, et al. A step forward for the undulation pump total artificial heart. *J Artif Organs* 2000;3:70–4.

Available online at www.sciencedirect.com
SCIENCE DIRECT®
Sensors and Actuators A 111 (2004) 304–309
SENSORS AND ACTUATORS A PHYSICAL
www.elsevier.com/locate/sna

# Three-axis magneto-impedance effect sensor system for detecting position and orientation of catheter tip

Kentaro Totsu [a,*], Yoichi Haga [b], Masayoshi Esashi [c]

[a] Department of Mechatronics and Precision Engineering, Tohoku University, 01 Aza-Aoba, Aramaki, Aoba-ku, Sendai 980-8579, Japan
[b] Department of Bioengineering and Robotics, Tohoku University, 01 Aza-Aoba, Aramaki, Aoba-ku, Sendai 980-8579, Japan
[c] New Industry Creation Hatchery Center (NICHe), Tohoku University, 01 Aza-Aoba, Aramaki, Aoba-ku, Sendai 980-8579, Japan

Received 29 December 2002; received in revised form 18 November 2003; accepted 20 November 2003

**Abstract**

A catheter-based minimally invasive therapy requires real time information about the position and orientation of a catheter tip for safe operation. To decrease X-ray exposure and to provide 3D information for operators, a simple sensor system for detecting the position and orientation utilizing the earth's magnetic field and ac (10 kHz) magnetic field transmitted by a two-axis source coil is proposed. A 2 mm × 2 mm × 3 mm three-axis MI sensor (Magneto-Impedance effect sensor) fabricated on a polymer structure for measuring the earth's magnetic field and the ac magnetic field is mounted on the catheter tip. The advantages of this sensor are: (1) small size; (2) high sensitivity; (3) retaining of through hole. The position and orientation is calculated and the obtained information of the position and orientation of the catheter tip is superimposed on the 3D map of the blood vessel captured in advance. A measurement in a blood vessel model has been performed and the calculated position and orientation image has been superimposed on the 3D graphic image of the blood vessel. The sensor system obviously indicated where the catheter tip was in the "y" shape blood vessel model.


*Keywords:* MI sensor; Catheter; Navigation; Position and orientation; 3D

## 1. Introduction

A catheterization used for the minimally invasive therapy has been widely carried out. Doctors can access to diseased area via blood vessel by insertion of a catheter and can do therapy with minimally invasion. In the therapy using the catheterization, real time information about the position and orientation of a catheter tip is necessary for safe navigation in the blood vessel. Generally, X-ray radioscopy is used to monitor the position and orientation of a catheter. However X-ray radioscopy can provide only two-dimensional (2D) images and requires an X-ray shielded room. Besides doctors must put on a heavy protector during the procedure and a long time X-ray exposure is harmful to patients and medical staff. As blood vessel is distributed three-dimensionally, it is helpful for navigation of a catheter if 3D image can be obtained. And navigation system without X-ray exposure is preferable for patients and doctors. In order to detect a three-dimensional (3D) position and orientation of an object, magnetic, optic, ultrasonic and mechanical sensors are mostly employed. A lot of magnetic detecting systems have already developed and commercialized [1–9]. The magnetic detection systems have some advantages.

1. Disturbance of magnetic field in a human body can be ignored because the permeability of human body is nearly equal to 1, which is equal to the permeability of the air.
2. A magnetic field is regarded safe if appropriate frequency and intensity are used.
3. A miniaturization of a magnetic sensor is relatively easy.

A magnetic position and orientation detecting system has been commercialized for monitoring the shape of an endoscope [7]. The coils are built in the endoscope and transmit magnetic fields. The outer diameter of the endoscope is about 12 mm. The other application is electrophysiological mapping and positioning of the site for RF catheter ablation in a heart [8,9]. The coils are built in the catheter tip and detect magnetic fields transmitted by external source coils. However the outer diameter of the tip is relatively small (3 mm), there is no through hole for inserting micro tools (e.g., guide wire) and injection of contrast medium and drug. In this paper, a simple real time catheter navigation system using a small three-axis magneto-impedance effect sensor, with less

* Corresponding author. Tel.: +81-222176937; fax: +81-222176935.
*E-mail address:* totsu@mems.mech.tohoku.ac.jp (K. Totsu).

0924-4247/$ – see front matter © 2003 Elsevier B.V. All rights reserved.
doi:10.1016/j.sna.2003.11.018

X-ray exposure during a catheterization is proposed. The sensor system can be applied to not only a catheter but also other small tools for minimally invasive therapy, such as an endoscopic procedure.

## 2. System concept

Fig. 1 shows the proposed catheter navigation sensor system. Before a catheterization, 3D image data of the blood vessel of a patient is captured by X-ray CT or MRI and is stored in a computer. During the catheterization, the position and orientation of the tip of the catheter is detected by a magnetic sensor built in the tip of the catheter. A cursor which indicates the position and orientation of the catheter is superimposed on the 3D internal image of the human body (e.g., blood vessel). This system can be useful for 3D navigation in other organs and tracts, e.g. branches of bronchus, digestive systems (stomach, duodenum, colon) and urinary tract for more precise operation in the human body.

If this sensor system is compared to a commercialized car navigation system, a catheter tip corresponds to a car and blood vessels correspond to roads. An operator can control the catheter tip in blood vessel as if the operator drives a car on the road.

As shown in Fig. 1, the sensor composed of three orthogonal magnetic sensor elements detects the earth's magnetic field as a dc field and ac (10 kHz) magnetic fields transmitted by a two-axis source coil placed near the patient. A 3D orientation of the sensor is represented by three Euler's angles [10]. A measurement of the earth's magnetic field is used to obtain two of Euler's angles, measurements of two ac magnetic fields are used to obtain the remaining one of Euler's angles and a 3D position of the sensor [11].

## 3. Sensor

### 3.1. Principle of sensor

Concerning the sensor characteristics, the three-axis magnetic sensor detects the earth's magnetic field and the ac magnetic field simultaneously to achieve the algorithm, and the size of the sensor should be less than 2 mm in order to built in a catheter. In several magnetic sensors, Magneto-Impedance effect sensor (MI sensor) has received attention recently because of its high sensitivity ($10^{-10}$ T), high response speed (MHz), low power consumption (10 mW using CMOS IC) and small size (1~2 mm) [12,13]. Therefore the MI sensor was selected for our sensor system. The MI sensor utilizes an electromagnetic phenomenon in which an impedance $Z$ of electrically conductive magnetic materials magnetized with a high frequency current inducing the skin effect is sensitively changed with an applied external magnetic field (MI effect) [12]. As the sensor head, an amorphous wire type is often used because of its high sensitivity compared to a thin film type. The impedance $Z$ of a wire of the MI sensor head is expressed as [12]

$$|Z| \approx \frac{a}{2\sqrt{\rho}} R\sqrt{\omega\mu_\theta}$$

where $a$ is a radius, $l$ a length, $\rho$a resistivity, $\mu_\theta$ a circumferential permeability magnetized with a sinusoidal current with angular frequency $\omega$ and $R = \rho l/\pi a^2$ is the dc resistance.

If the impedance $|Z|$ is measured, intensity of the external magnetic field can be detected because the $\mu_\theta$ is sensitively changed by the external magnetic field parallel to the MI sensor.

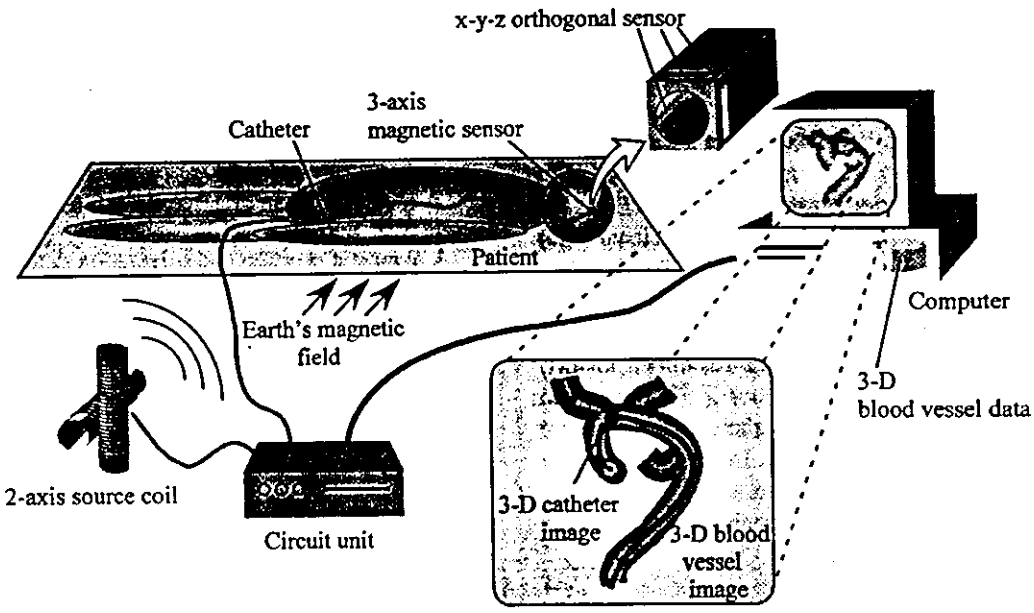


Fig. 1. Schematic of sensor system.

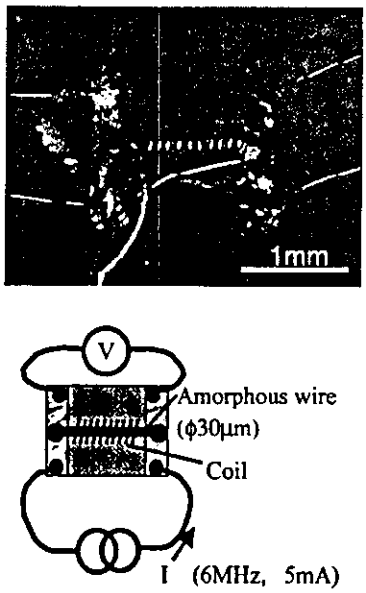


Fig. 2. Structure of MI sensor.

### 3.2. Fabrication of sensor

A MI sensor as a test type was fabricated as shown in Fig. 2. A FeCoSiB amorphous wire of 30 μm in diameter and of 1.5 mm in length was fixed at the center of a glass epoxy substrate and electrically connected to electrodes by using conductive epoxy. The four lead wires were also connected to the electrodes by soldering to pass current (6 MHz, 5 mA) and to detect voltage between the both sides of the amorphous wire to measure impedance of the wire. In order to apply a bias magnetic field, the amorphous wire is surrounded by a small coil. To transfer the signals, ultra-small diameter coaxial cables (Sumitomo Electric Industries 44110T) of 250 μm in outer diameter, and of 1 m in length were used between the sensor and the circuit. A 6 MHz sinusoidal voltage modulated at 10 kHz equal to the frequency of the transmitted ac magnetic field was obtained and processed at the circuit. The characteristics of the sensor using a differential amplifier is shown in Fig. 3. The impedance curve has assumed a minimum at 0 T without bias coil current. As the bias coil current shifts the impedance curve, polarity of the external dc magnetic field can be determined.

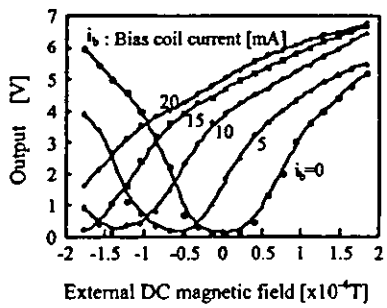


Fig. 3. Characteristics of MI sensor with changing of bias coil current.

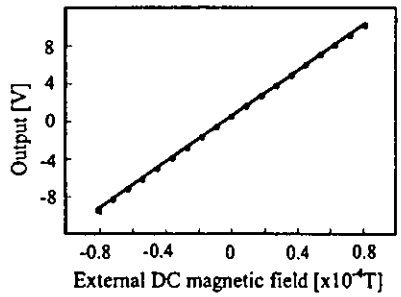


Fig. 4. Characteristics of MI sensor for external dc magnetic field.

In the circuit, the signal processing was carried out as follows: (1) differential amplification; (2) detection by using a diode; (3) smoothing by using capacitors; (4) separation of AC(10 kHz) component and DC(earth's magnetic field) component; (5) negative feedback of a output of the dc component to the passing current of the bias coil to improve linearity.

In order to determine a direction of the sensor, phase of the ac magnetic field was detected. Therefore 10 kHz current synchronized to the ac magnetic field passed the bias coil as AC bias current. If the detected signal and the bias current are in phase, the output of the circuit is positive. If they are out of phase, the output of the circuit is negative. The result of a measurement of dc magnetic field and ac magnetic field are shown in Figs. 4 and 5 respectively. High sensitivity and high linearity have been achieved.

A three-axis MI sensor was fabricated by integration of three MI sensors on a polymer structure by using epoxy glue as shown in Fig. 6a And the sensor was covered with silicone rubber tube as shown in Fig. 6b. Precise orthogonal alignment of the three MI sensors was required to decrease interference between three-axis components. A polymer structure which had three grooves and patterned electrodes was used to eliminate alignment error of the three orthogonal sensors and to make fabrication easy. The size of the polymer structure was 2 mm × 2 mm × 3 mm. A through hole at the center of the structure is used for inserting micro tools (e.g., guide wire) or injection contrast medium and drug. The structure was fabricated by machining and the electrodes were formed by electro-less plating. In the future, a cheaper polymer

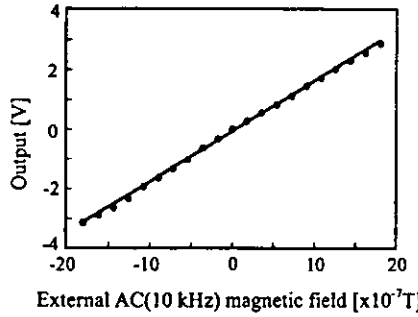


Fig. 5. Characteristics of MI sensor for external ac (10 kHz) magnetic field.

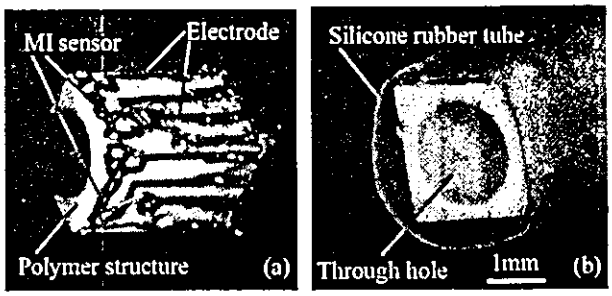


Fig. 6. Fabricated three-axis MI sensor on polymer structure: (a) and covered with silicone rubber tube (b).

structure can be obtained as the base structure of the sensor by using injection molding. A smaller size three-axis MI sensor without a through hole has been also fabricated as shown in Fig. 7. The size of the sensor is 1 mm × 1 mm × 1 mm. These small three-axis MI sensors can be placed in small medical tools (e.g., a guide wire and the tip of the forceps).

### 3.3. Sensor system

The sensor system is shown in Fig. 8. The output signal transferred from the three-axis MI sensor was processed at the circuit and acquired by a computer via an analog-digital converter. A function generator sent dc biased 10 kHz signal to the circuits for sensing and also sent 10 kHz signal to the source coils via a MOS switch and amplifiers. The MOS switch was controlled by digital signal transmitted from the computer via a digital output port. A two-axis solenoid was fabricated as the source coil. The length and diameter of each axis coil were 10 mm and 40 mm respectively. The coil was composed of a ferrite core and insulated cupper wire. A capacitor was put in parallel to make a resonant circuit at 10 kHz. An application program was built for control the sensor system, calculation based on the algorithm and indication the position and orientation.

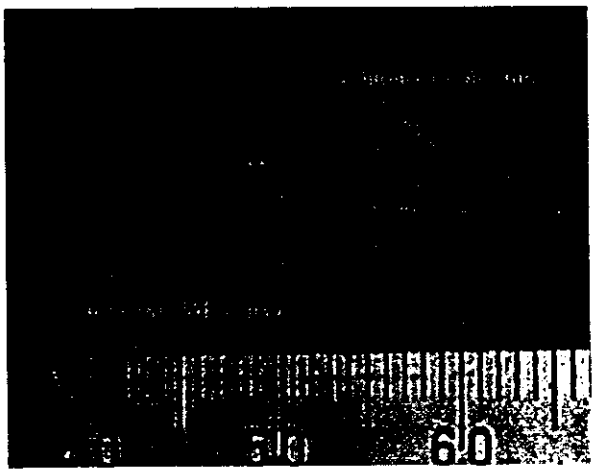

Fig. 7. Fabricated 1 mm size three-axis MI sensor.

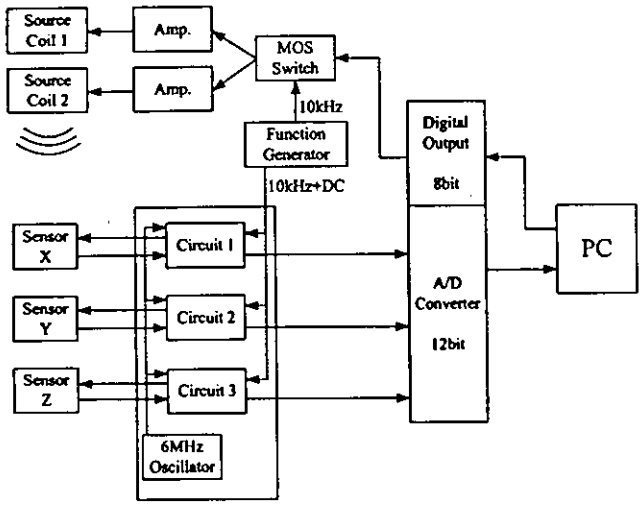


Fig. 8. Configuration of sensor system.

## 4. Experimental results

The resolution and the error of 3D position and orientation of the developed sensor system were measured. For a position measurement, the three-axis MI sensor was put on a plane parallel to the coordinate of the source coil. The measurement area was 100 mm × 100 mm. The mean of the position error was 2 mm. The maximum 3D position error of 5 mm was occurred and the resolution of the 3D position was about 0.4 mm around the center area and 1.0 mm around the marginal area respectively. The orientation of the sensor was regarded as a constant when position measurement was performed. An orientation measurement has been also performed. The mean of the rotation angle error of 9° was occurred when the MI sensor was turned 360° on the vertical axis. The resolution was about 1°.

A measurement was performed in a blood vessel model. The model consisted of polymer tubes of which outer

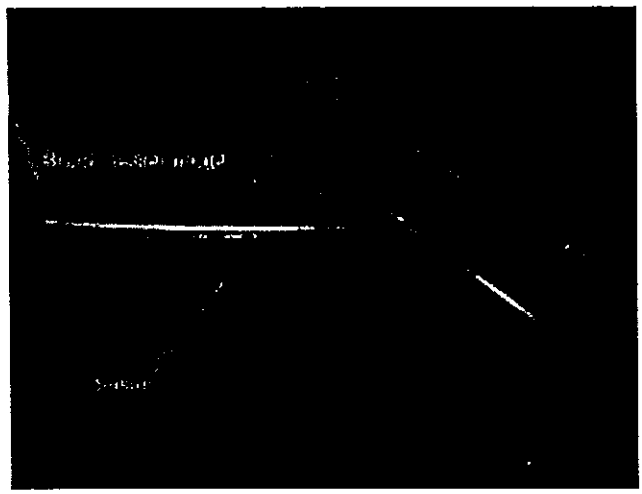

Fig. 9. "y" Branch shape of blood vessel model with inserted three-axis MI sensor.

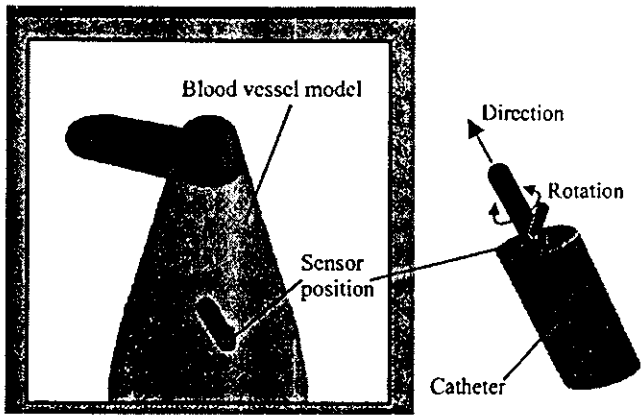


Fig. 10. Sensor position and orientation image superimposed on 3D image of blood vessel model.

diameter and internal diameter are 6 mm and 4 mm respectively as shown in Fig. 9. At the middle point of a tube of 100 mm in length, the other tube was connected for making a "y" branch shape of a blood vessel. The model was placed 100 mm apart from the source coil. A calculated position and orientation image were superimposed on 3D computer graphics of the blood vessel model on a display as shown in Fig. 10. The large bar (black) indicates the direction and the small bar (gray) indicates the rotation around the axis of the catheter respectively. The sensor position can be confirmed on a 2D image as shown in Fig. 11. The sensor was inserted and moved repeatedly in the vessel model and the position and orientation were continuously monitored. The sensor system successfully indicated whether the catheter tip was in the vessel branch or straight part of the vessel on 3D image. A desirable viewpoint and a magnification can be selected using console on the monitor. The mean of axial position error was about 2 mm. The performance of the fabricated smaller three-axis MI sensor (1 mm × 1 mm × 1 mm) was the same for the 2 mm × 2 mm × 3 mm sensor.

## 5. Discussion

It was considered that the position and the orientation measurement error were mainly caused by distorted distribution of the ac magnetic field transmitted from the source coil, which differ from the ideal distribution. In order to achieve more accurate measurement, the source coil should be precisely designed and fabricated. The measurement area could be extended by using additional source coils. When a magnetic material is placed between the source coil and the sensor, the magnetic field is disturbed and compensation of the magnetic field is difficult. When a non-magnetic metal is placed between the source coil and the sensor, the magnetic field is also disturbed because of eddy current. In this case, the disturbance will be reduced by utilizing pulse magnetic fields instead of the ac magnetic fields. While considering disturbance of the earth's magnetic field in the whole measurement area, it can be compensated if additional sensor is used as a fixed reference sensor to monitor the earth's magnetic field during the measurement. For clinical use, because of movements of a patient after image acquisition, it is necessary to consider difference between the stored image acquired before the operation and the real time image. In this case, additional capturing of 3D image might be required. As our three-axis MI sensor is small and sensitive and also retains through hole, it can be adapted to several medical micro tools, e.g. endoscopes, forceps, RF coagulators and

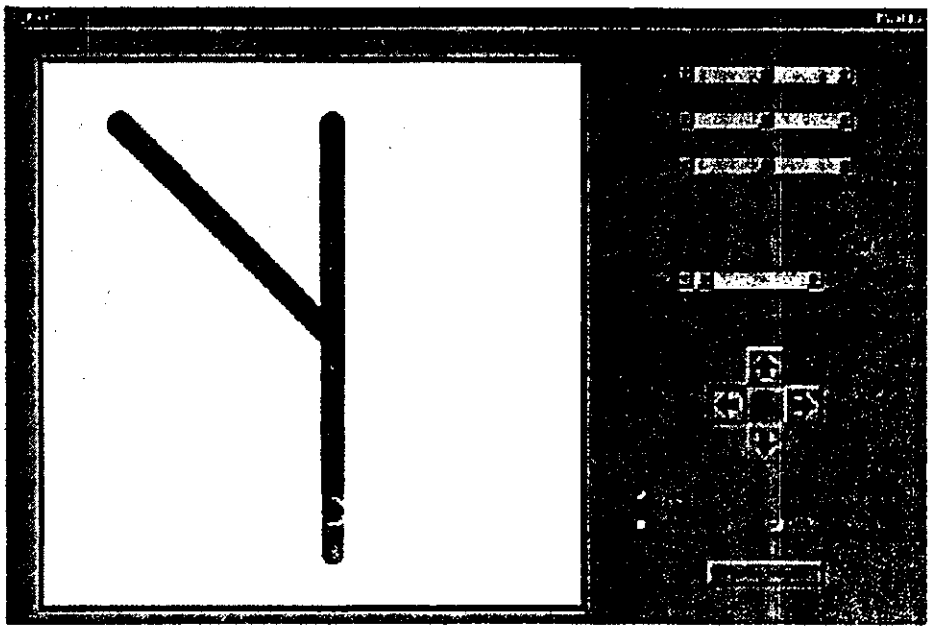

Fig. 11. Sensor position image (black point) superimposed on 2D image of blood vessel model.

laparoscopic micro tools. Another effective medical application of the position and orientation sensor is functional mapping in the human body for example electrophysiological mapping in a heart [8,9].

## 6. Conclusion

We have developed a three-axis MI sensor system for monitoring the position and orientation of a catheter tip. A novel 3D catheter navigation system using the three-axis MI sensor and 3D internal image of human body has been proposed. The three-axis MI sensor of 2 mm × 2 mm × 3 mm and 1 mm × 1 mm × 1 mm which can be mounted at the tip of the catheter have been developed. The resolution of the position and orientation were 1 mm and 1°, respectively. Detection in blood vessel model has been performed and the position and orientation of the catheter tip is displayed as an indicator on the 3D computer graphics of blood vessel.

## Acknowledgements

The authors gratefully acknowledge Prof. K. Mohri (Nagoya University) and Prof. H. Matsuki (Tohoku University) for enligtening advices and discussions. The authors would like to thank Sumitomo Electric Industries, Ltd. and Unitika Ltd. for supplying the ultra-small diameter co-axial cable and the amorphous wire, respectively. This work was supported in part by Micro Machine Center and a Grant-in-Aid (No. 10359001 ) from the Ministry of Education, Culture, Sports, Science and Technology of Japan.

## References

[1] F.H. Raab, E.B. Blood, T.O. Steiner, H.R. Jones, Magnetic position tracker, IEEE Trans. Aerospace Electron. Sys. AES-15 (5) (1979) 709–717.
[2] M. Takayama, K. Maenaka, A. Yamamoto, Position Sensing System Using Integrated Magnetic Sensors And Neural Networks, in: Digest of Technical Papers of Transduccers'01, Munich, Germany, 2001, pp. 76–79.
[3] S. Yabukami, H. Kikuchi, M. Yamaguchi, K.I. Arai, K. Takahashi, A. Itagaki, N. Wako, Motion capture system of magnetic markers using three-axial magnetic field sensor, IEEE Trans. Magn. 38 (2000) 3646–3648.
[4] J.B. Kuipers, SPASYN—an Electromagnetic relative position and orientation tracking system, IEEE Trans. Instrum. Measure. IM-294 (1980) 462–466.
[5] D. Tanase, N.H. Bakker, D.van Loon, J.F.L. Goosen, P.J. Trimp, J.A. Reekers, P.J. French, Radiation dose reduction in minimally-invasive intravascular procedures using a magnetic guidance system, in: Proceedings of Second Annual International IEEE-EMBS Special Topic Conference on Microtechnologies in Medicine & Biology, Madison, Wisconsin, USA, 2002, pp. 305–308.
[6] J.S. Bladen, A.P. Anderson, G.D. Bell, D.J. Heatley, A non-radiological technique for the real time imaging of endoscopes in 3 Dimensions, 1993 IEEE conference record, Nucl. Sci. Symp. Med. Imag. Conf. 3 (1993) 1891–1894.
[7] http://www.olympus.co.jp/LineUp/Endoscope/upd.html.
[8] L. Gepstein, G. Hayam, S.A. Ben-Haim, A novel method for non-fluoroscopic catheter-based electroanatomical mapping of the heart, Circulation 95 (6) (1997) 1611–1622.
[9] S. Shpun, L. Gepstein, G. Hayam, S.A. Ben-Haim, Guidance of radiofrequency endocardial ablation with real-time three-dimensional magnetic navigation system, Circulation 96 (6) (1997) 2016–2021.
[10] R.P. Paul, Robot manipulators: mathematics, programming, and control: the computer control of robot manipulators, MIT Press, Cambridge, USA, 1981.
[11] K. Totsu, Y. Esashi, M. Haga, Magnetic sensor system for detecting position and orientation of a catheter tip, Trans. IEEJ 120-E (5) (2000) 211–218 (in Japanese).
[12] K. Mohri, T. Uchiyama, L.V. Panina, Magneto-Impedance (MI) Micro Magnetic Sensors—Principle and Applications-, in: Digest of Technical Papers of Transduccers'99, Sendai, Japan, 1999, pp. 76–79.
[13] K. Mohri, T. Uchiyama, L.P. Shen, C.M. Cai, L.V. Panina, Sensitive micro magnetic sensor familiy utilizing magneto-impedance (MI) and stress-impedance (SI) effects for intelligent measurements and controls, Sens. Actuators A 91 (2001) 85–90.

## Biographies

*Kentaro Totsu* was born in Kanazawa, Japan, on March 15, 1977. He received his BE and ME degrees in mechanical engineering from Tohoku University in 1999 and 2001, respectively. He is currently pursuing his PhD in mechanical engineering at Tohoku University in which his research concentrates on MEMS-based medical sensors and measurement systems.

*Yoichi Haga* was born in Sendai, Japan, on April 4, 1965. He received his MD from Tohoku University School of Medicine, in 1992. From 1994 to 1996, he was with Tohoku Kosei-Nenkin Hospital. From 1996 to 2002, he was a research associate in the Department of Mechatronics and Precision Engineering, Tohoku University. He received his PhD degree from Graduate School of Engineering, Tohoku University in 2002. He is currently an assistant professor at the Department of Bioengineering and Robotics, Tohoku University. He has been studying micromachining and nanomachining for medical and welfare application (mainly minimally invasive diagnosis and treatment).

*Masayoshi Esashi* was born in Sendai, Japan, on January 30, 1949. He received his BE, ME and Doctor of Engineering degrees all in electronic engineering from Tohoku University, in 1971, 1973 and 1976, respectively. From 1976 to 1981, he served as a research associate at the Department of Electronic Engineering, Tohoku University and he was an associate professor from 1981 to 1990. He was a professor at the Department of Mechatronics and Precision Engineering from 1990 to 1998. Since 1998, he has been a professor at the New Industry Creation Hatchery Center (NICHe), Tohoku University. He was the director of the Venture Business Laboratory in Tohoku University from 1995 to 1998. He is also an associate director of the Semiconductor Research Institute. He has been studying micro-sensors and integrated micro-systems. His current research topic is a micro-technology for saving energy and natural resources. He is a member of the IEEE and the IEE of Japan.

総　説

# ナノテク集積人工心筋開発プロジェクト

山家智之*，白石泰之*，井口篤志**，田林晄一**
芳賀洋一***，江刺正喜***，吉澤　誠***，田中　明***
松木英敏***，佐藤文博***，川野恭之****，羅　雲****
高木敏行****，早瀬敏幸****，圓山重直****，王　慶田*
段　旭東*，仁田新一*，岡本英治*****
久保　豊******，大坂元久*******，梅津光生********

**研究要旨**

東北大学では，先端的ナノテクを集積することにより，人工心臓や補助人工心臓とは全く異なる新しい補助循環装置である「人工心筋」を開発するプロジェクトに着手した．システムは血行動態を感知するナノセンサ，人工心筋の駆動制御を行うナノマイクロチッププロセッサ，経皮エネルギー伝送システムならびにエレクトロハイドローリックアクチュエータからなる．日本人とほぼ同じ体重を持つヤギを用いて動物実験にも成功し，次年度以降の慢性実験での心補助効果確認並びに耐久性試験へ進み，臨床前試験へのステップへ進む予定である．

**キーワード：ナノテク人工心筋，ナノセンサ，ナノマイクロプロセッサ**

## 緒　言

東北大学の医工学連携研究プログラム：バイオナノテクノロジー基盤未来医工学は，文部科学省の21世紀COEプログラムに選択された．この研究計画では主として医工学研究者の養成に重点がおかれ，研究にはほとんど予算を用いることはできないが，教育を介してますます学内の連携を深め，メディカルエンジニアリング研究を進める機運が張りつつある．

加齢医学研究所も21世紀COEの事業推進担当に採択されているが，この21世紀COEでは，研究費はそれぞれの事業推進担当者が独自に競争的資金を獲得して研究を進めることが強く求められている．東北大学では，厚生労働省の萌芽的研究推進事業などによりナノテクを集積した人工臓器開発，ドラッグデリバリーシステム開発などを推進している．

不可避的に到来する高齢化社会においては心不全などのハンディキャップを持つ高齢者の社会復帰も強く望まれることになる．特に重症心不全では人工心臓か心臓移植しか救命の方法論はありえないが，移植臓器の不足は深刻で人工心臓への期待は大きくなりつつある．しかしながら，現在欧米で開発されているシステムは日本人に埋め込むには大きすぎることは定説になっている．

原点に返って考察してみれば，循環を補助するのに心臓を丸ごと摘出したりポンプを埋め込む必要は必ずしもない．救急における心臓マッサージの原理を考察すれば，心臓は外から圧縮することにより比較的容易に拍出を維持できうることは広く知られた事実である．開胸心マッサージにおいては，心臓を手で握ることにより，十分な血圧と血液循環が得られている．

*東北大学加齢医学研究所病態計測制御
**東北大学大学院医学系研究科心臓血管外科
***東北大学大学院工学研究科
****東北大学流体科学研究所
*****北海道東海大学工学部情報システム学科
******東京女子医科大学附属第二病院内科
*******日本医科大学老人病研究所
********早稲田大学理工学部機械工学科

本研究の目的は，心臓を押すことにより心拍出を維持する全く新しい心室補助装置の開発である．東北大学で開発中のナノセンサを駆使して心筋の機能と血行動態を探知し，マイクロ制御チップで補助循環の必要性を計算するインテリジェント制御機構を持つ超小型の埋込型心室補助装置を開発し，心不全に苦しむ患者に，簡単にアプリケーションが可能な超小型デバイスをナノテクの応用により開発する．

開発される心室補助装置は，人工心臓のように常に拍動していなければ血栓形成の危険のあるポンプシステムではなく，必要なときに必要なだけアシストするデバイスであるので耐久性も大きく期待される．ここで開発される制御メカニズムは人工心臓だけでなく様々な人工臓器へ応用が可能であり，また内外で開発中の人工心臓にも新しいアプリケーションとして応用できる汎用性の高いものである．

### B．研究方法

本研究で開発する心室補助装置は超小型アクチュエータで心筋の拍動を補助するシステムであり，心臓の外面に縫着されるので従来の人工心臓のように血栓の危険もなく，人工弁の耐久性の問題もない．必要がない時は自己心の収縮に任せるので耐久性の向上も期待されメカニズムがシンプルなので小型軽量化も可能である．

アクチュエータとしては，比較的軽症の患者のためには現在，特許申請中の形状記憶合金・形状記憶樹脂を用いたマイクロマシン化が可能なペルチェ運動素子（特願平11292727）を第1の候補にしている．(図1)

より重症の左心不全患者のためにはモータ駆動型も開発の視野に入れている．(図2)

最終的には，心室補助装置自体のナノマシン化も目標とする．

実験に当たっては東北大学加齢医学研究所動物実験倫理委員会の厳密な審査を受け，規定に従って実験を行った．

### 結　　果

第1にダイレクトドライブ方式の人工心筋開発を目指して動物実験を行った．そのためにできるだけ小型のものが望まれたので，ペルチェ運動素子を用いた動物実験を試みた．(図3)

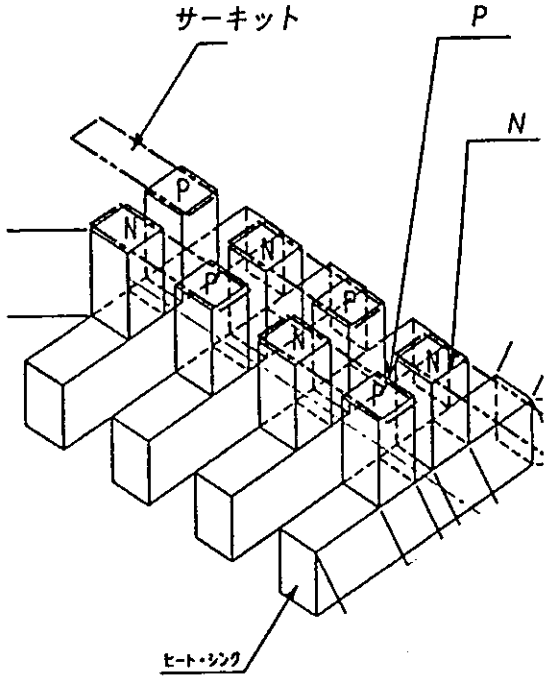


図1　ペルチェ運動素子

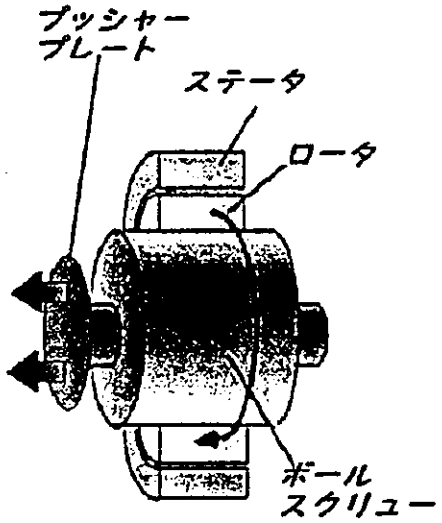


図2　ボールスクリューモータ型アクチュエータ

その結果，ペルチェ運動素子にて1Hzを超える駆動スピードが得られた．通常の形状記憶合金単体では0.1Hz前後の駆動スピードが限界であり，飛躍的駆動スピードの向上が具現化し，人工心筋への応用の可能性が大きく開けた．

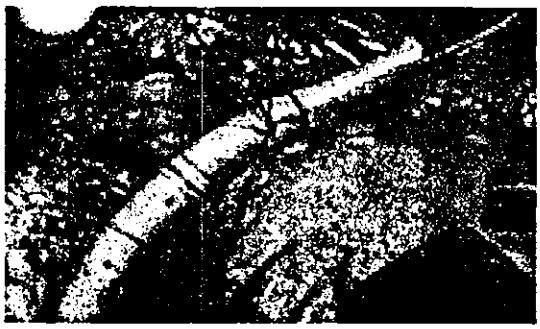

図3　ベルチェ運動素子動物実験

しかしながら，棒状の形状記憶合金によるベルチェ運動素子を心筋にダイレクトに縫い付けた結果，収縮時に，心筋の長軸方向から横にねじれてしまう現象が観察され，ダイレクトに収縮補助に結びつけるためには，解剖学的に心筋の走行に従う方向性を持った逢着が不可欠であるものと考えられた．

心筋の走行は解剖学的に三冠に別れ，それぞれが機能性を持って全体の収縮性に貢献していることが知られている．心筋梗塞患者では部位や場所によって様々な障害を受けることが報告されているので，解剖学的に最適の方向性に縫い付けて病態生理学的に有効な拍出が得られる可能性が示唆されたものと思われる．

次に広範囲の心筋梗塞患者及び拡張型心筋症患者のために，図2のボールスクリューモータによるダイレクトドライブを試みた．

人工心筋を開発するためにはソフィスティケイトされた方法論で心臓にアクチュエータを固定する必要がある．(図4)

心臓の手術時には緊急事態がよく起こり得るが，最近スタンダードになりつつある心拍動下の冠動脈バイパス手術などにおいては，虚血に晒されてきた心臓に負担をかける手術になりながら，体外循環を行っていないので，ふとした弾みに心室細動から心停止に至る可能性は非常に高く難易度も高い．

このような緊急時に簡単にアプリケーションすることができる人工心筋システムが存在すれば，臨床的にもその意義付けは極めて大きなものがある．

そこで考案されたのが図に提示する心室カップである．

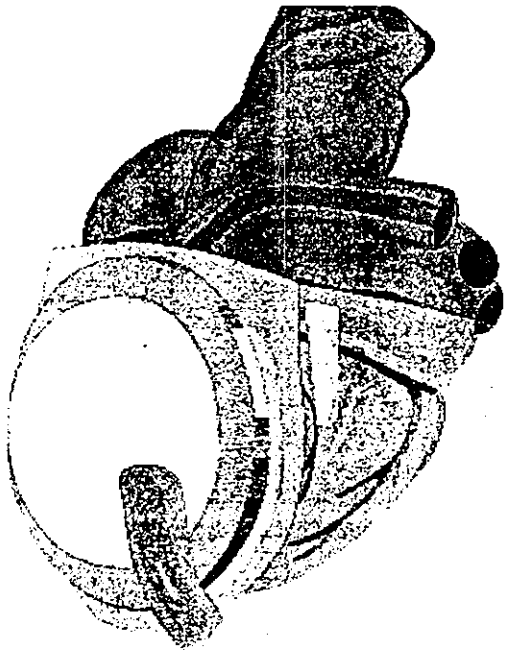

図4　心室カップ

手術中のアクシデント的な心停止の場合でも，速やかに心室に装着することが可能である．

日本人成人男性の平均体重とほぼ同様の体重を持つ成ヤギを用いた動物実験において予備実験的にポリカーボで試作した心室カップを装着してみたところ，ほぼ三秒以内に装着が可能であった．

人間は心停止してから3分以内に回復できなければ脳虚血から不可逆的な変化を経て意識が回復しないということは心臓発作の多い欧米からの報告でもよく言われてきているが，三秒以内に装着できるデバイスがあれば，手術中といえどもその意義は果てしなく大きい．

麻酔のアクシデントや出血性ショックなど，手術中には様々なアクシデントがいつでも起こり得ることは自明であり最悪の場合患者は不幸な転機を取る．

それを予防できうる簡便なデバイスがあればその応用範囲は無限とも言える展開を見せるであろうことは間違いない．(図5)

しかしながら問題点としては心室の拡張能が阻害されることで，肥大した心臓などでは心筋カップを嵌めると若干の拡張障害により動脈圧の減少傾向が認められる症例も存在した．(図6)

そこで次の展開としては拡張能力を保持したま

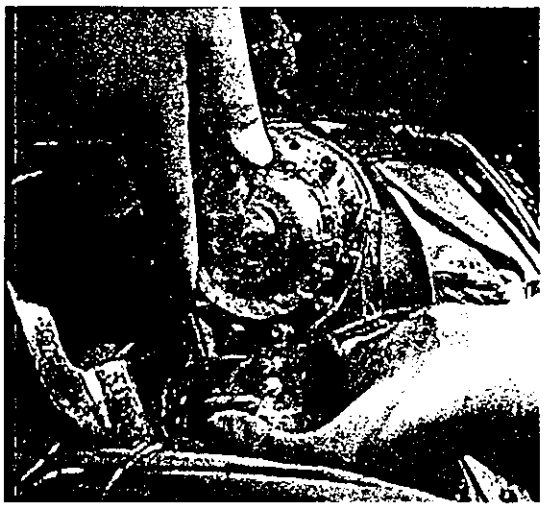

図5 動物実験中の心室カップ

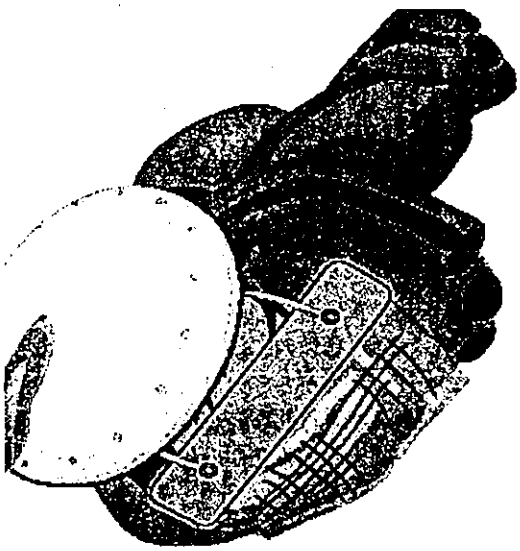

図6 バンド固定方式

まで固定が可能であるバンド方式なども検討した.

動物実験の結果では，心室カップ方式で認められた拡張障害による動脈圧の低下傾向は観察されず，人工心筋デバイスの作動により有意の心補助効果が確認されている.

しかしながら，ボールスクリューモータのダイレクトドライブ方式では，小柄なヤギの場合，胸腔スペースに不自由する場合もあり，更なる小型化の必要性が示唆された．特にボールスクリューモータでは，ストローク分の軸の長さが，反対方向へも突出してしまうのでこの問題は深刻である.

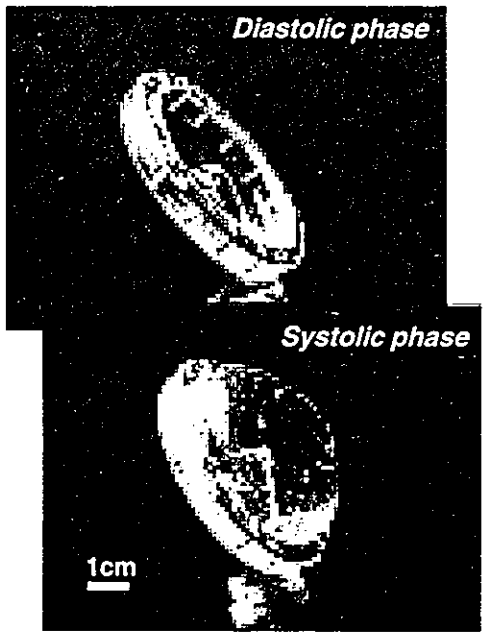


図7 エレクトロハイドローリック人工心筋

そこで考案されたのがエレクトロハイドローリック方式への新たな展開である．(図7)

ナノテク集中型の心室補助装置を目指してエレクトロハイドローリック方式の人工心筋開発を試みた.

このシステムのコンセプトは，アクチュエータを胸腔の外に置くことで，胸腔のスペースを節約できる．(図8)

アクチュエータは肋間に置き胸壁のスペースを有効活用する．アクチュエータの駆動エネルギーはシリコンオイルを介してダイアフラムを駆動し,心室を心マッサージの原理で押すことになる.

駆動エネルギーは経皮エネルギー伝送システムによって体外から供給される．東北大学で開発が進められている経皮エネルギー伝送システムは，外面をアモルファスファイバーで磁気シールディングしてあることに特徴がある.

磁気のシールディングは技術的になかなか困難ではあるが東北大学では独自技術でこれに成功し，外側への漏れ磁力を軽減することで世界最高級の伝送効率を具現化した．(図9)